PCCP

Accepted Manuscript

ROYAL SOCIETY OF CHEMISTRY

www.rsc.org/pccp

Electronic and Magnetic Properties of Honeycomb Transition Metal Monolayers: First-principles Insights

Xinru Li, Ying Dai*, Yandong Ma, and Baibiao Huang

School of Physics, State Key Laboratory of Crystal Materials, Shandong University, Jinan 250100, People's Republic of China

Abstract

P-electron-based monolayer materials have dominated the research of Dirac fermions since the first exfoliation of graphene. In the present work, the electronic and magnetic properties of *d*-electron-based Dirac systems are studied by combining first-principles with mean field theory and Monte Carlo approaches. From first-principle calculations, we demonstrate that transition-metal (TM) monolayers (TM = Ti, Zr, Hf, V, Nb, Ta), *d*-electron-based materials, could also hold Dirac cones not only *p*-electron-based materials as known before. This may shed light on breakthrough of new nanomaterials with d-type Dirac points. Moreover, the carrier mobility near the Dirac points of these materials can be tuned regularly by isotropic strains from -5% to 5%, without breaking the Dirac cones. However, the Dirac points would disappear under anisotropic strains, indicating that rigorous honeycomb lattice may be main precondition for Dirac points in TM-monolayers. Furthermore, some TM-monolayers (TM = Ti, Zr, Hf) exhibit ferromagnetic couplings simultaneously. In addition, by mean field theory and Monte Carlo methods, it is found that the Curie's temperatures of TM-monolayers can be higher than 580 K even to 1180 K. Our

* E-mail: daiy60@sina.com

findings significantly expand the Dirac systems.

I. Introduction

Since graphene was discovered, two-dimensional (2D) systems have been the focus of recent research efforts [1-3]. Following graphene, new 2D materials have been realized and many more have been predicted, such as silicene, hexagonal boron nitride, ZnO, MoS_2, as well as graphene derivatives [4-8]. Nevertheless, graphene is still drawing most of the attention because of its fascinating electronic properties. These unusual electronic properties are derived from its planar honeycomb structure, bringing out special Dirac points and cones near Fermi level. And the curvature approaching Dirac point along certain symmetry-determined directions is zero, which mimic massless and high performance Dirac fermions [9]. The existence of Dirac points provides widely application in electronics because of its linear band dispersion and high carrier mobility [10,11]. Except for graphene, other materials such as, silicene and graphyne, have been found or predicted to be with similar Dirac points [12-14]. However, all of these Dirac systems mentioned above are derived from *p* electrons, which can be called *p*-type Dirac points. To date, no other type (i.e., *s*-type or *d*-type) Dirac systems have been studied systematically. This limitation hampers the application of Dirac points into many aspects such as novel quantum behaviors and spin orbit coupling systems. Thus, searching for new nanomaterials with Dirac points contributed by s or *d* electrons is still an arduous task for researchers.

On the other hand, other than intrinsic Dirac point properties, magnetic behavior is another criterion to measure performance of nanomaterials in some practical

applications such as magnetic storage and record, memory components and magnetic card [15,16]. In most of existing pristine 2D materials, rare magnetic ordering is expected except for VX_2 (X= S, Se) [17,18]. Traditional alternative approaches of magnetic modulation are introducing point defects, magnetic atoms, and adsorbing nonmetal elements [19-21]. However, the prior methods to introduce magnetism is somewhat tough to control experimentally. Therefore, exploring novel 2D monolayer materials with intrinsic ferromagnetism is essential for integrated spintronics devices.

Very recently, new novel 2D honeycomb-like monolayer，such as Hf monolayer and single-layered Rh nanosheet has been synthesized experimentally [22, 23]. Experimental characterization reveals that Hf-monolayer is a planer structure and has its own honeycomb lattice, morphologically identical to graphene. Moreover, simply first-principles calculations predicted that Dirac points exist in both spin-up and spin-down band structures [22], but the internal mechanism of the Dirac points and magnetic properties are not mentioned. That is to say, current understanding of this fascinating system is not sufficient enough. How about the performance of Dirac points in Hf-monolayer? What is the origin of Dirac points and ferromagnetism and how to tune it regularly? What temperature can Hf-monolayer withstand to maintain ferromagnetism? How about other analogous transitional metals if they can form honeycomb monolayer?

In this paper, we explore the electronic properties and magnetic behaviors of a series of transition-metal (TM) monolayers (TM = Ti, Zr, Hf, V, Nb, Ta) by means of density functional theory calculations (DFT). It is revealed that all these

TM-monolayers exhibit metallic and some of them have ferromagnetic coupling (TM = Ti, Zr, Hf). Most importantly, Dirac points contributed by *d* electrons are verified for the first time in both spin-up and spin-down states for all TM-monolayers. Isotropic strain can modulate magnetic moment and carrier mobility regularly without breaking Dirac points. Furthermore, we apply Ising model with mean field theory and Monte Carlo simulations to evaluate Curie's temperatures of ferromagnetic TM-monolayers, which is a powerful guidance for further application. Our work for novel TM-monolayers with d-type Dirac points may pave a way for the next generation of 2D nanoelectronics.

II. Computational Methods

All of our calculations, including geometry relaxation and electronic structure calculation, are based on the spin-polarized density functional theory (DFT) using generalized gradient approximation (GGA) for exchange-correlation potential [24]. The Perdew-Burke-Ernzerhof (PBE) functional was used for GGA as implemented in the Vienna *ab initio* Simulation Package (VASP) [25] [26]. For the geometric and electronic structural calculations, a supercell consisting of 2×2 unit cells of TM-monolayers is employed. A vacuum layer of 20 Å is adopted in the direction normal to the interface, representing the isolated slab boundary condition. The Brillouin zone is represented by the set of 11×11×1 k-points for the geometry optimizations and by that of 13×13×1 k-points for the static total energy calculations [27]. The energy cutoff, convergence in energy, and force are set to 450 eV, 10^{-5} eV, and 0.02 eV/Å, respectively. Particularly, in band structures calculations, a 1×1

supercell containing two TM atoms is adopted and two possible initial magnetic configurations are considered: one is the ferromagnetic (FM) state and the other is the antiferromagnetic (AFM) state. Thus, ground state of TM-monolayer is determined by lower total energy between FM state and AFM state.

III. Results and Discussion

3.1 Geometries

Firstly, geometric properties of the TM-monolayer are examined. The results show that the relaxed structures of such TM-monolayer are in analogy to pristine grapheme that with no buckling as shown in **Figure 1**. Detail optimized parameters of various TM-monolayer are listed in **Table 1**. For Hf-monolayer, which has been synthesized experimentally, the calculated distance between two adjacent Hf atoms in the 2D plane to be ($c/\sqrt{3}$) Å = 2.81 Å. Half of the value, 2.81 Å/2 =1.405 Å, is also within the range of the empirical covalent radii for Hf, which are between 1.21 and 1.52 Å. As we can see, the calculated bond lengths and lattice constants of TM-monolayers in the same period in periodical table increase monotonically as the atomic number increase from IV to V group. Such a trend is reasonable and can be understood from the perspective of electronegativity and atomic radius. In the same period, electronegativity of elements in group IV (IV-elements) is relatively weaker than that of elements in goup V (V-elements), while the atomic radius increase monotonically from IV-elements to V-elements. Weaker electronegativity and larger atomic radius are responsible for larger bond length and constant parameter.

3.2 Electronic structures and magnetic properties

Now a question arises as to whether the intrinsic electronic properties are similar to graphene with the similar geometry. It is known that for graphene, three of four valence electrons form bonds with neighboring carbons while the other one makes contribution to p_z states, which are roughly vertical to the layer plane, bind covalently with each other and develop into delocalized π and π^* states. Such bands are responsible for Dirac point and the linear band dispersion near Fermi level. While, the six TMs are prone to tetravalent states as graphene, we wonder if Dirac points contributed by *d* states can be formed in TM-monolayers. Therefore, six of TM-monolayers' spin-polarized band structures are calculated and displayed in **Figure 2**. Band structure information shows that all TM-monolayers are of metallic character. For TM-monolayers (TM = Ti, Zr, Hf), spin-down and spin-up states are not symmetrical, indicating that they exhibit magnetic properties. On the other hand, the other three TM-monolayers are nonmagnetic with symmetrical spin-down and spin-up states. The differences arise from various ground states of different TM-monolayers in **Table 1**. As for TM-monolayers (TM = Ti, Zr, Hf), the total energies of FM states are lower than that of AFM states, which indicates that, in the three TM-monolayers, FM states are energetically more stable than AFM states. Thus, the total magnetic moments per unit cell are not equal to 0 μ_B and the corresponding spin-up and spin-down band structures are unsymmetrical. While for TM-monolayers (TM = V, Nb, Ta), the total energies of AFM states are smaller than (TM = V) or equal to (TM = Nb, Ta) that of FM states, according to thermodynamically stability, which results in 0 μ_B magnetic moments per unit cell and the corresponding spin-up and

spin-down band structures are symmetrical. More Surprisingly, not only Hf-monolayer which has been reported to own Dirac point at K point around Fermi level [22], but also all TM-monolayers have Dirac points at K point in both spin-down and spin-up states, as stressed out with black circles in Figure 2. It is worth to mention that other nodes throughout the band structures in TM-monolayers are examined to be parabolic instead of Dirac-type points with linear dispersion, which may make less contribution to transportation. These fascinating features prompt us to make further exploration.

As mentioned above, Dirac point is rare but precious properties and provide widely application in nanoelectronics and it is essential to evaluate the electronic behaviors near Dirac point. The Dirac cones of each TM-monolayers have been examined and all of them exhibit linear band dispersion. Take spin-down states of Hf-monolayer for example, more intuitive three dimensional band structures and partial density states for *d* orbitals around Dirac cones are shown in **Figure 3**. It should be noted that, the band structures near Dirac points are mainly contributed by dz^2 orbital in TM-monolayers, which is different from previous p-type Dirac points. As we know, for most of the previous studies, the Dirac points of the concerned 2D systems generally contributed by *p* electrons. So our work may shed light on breakthrough of new nanomaterials with d-type Dirac points.

Considering the current practical applications of 2D nanoelectronics, higher carrier mobility and linear band dispersion are very important. For all investigated TM-monolayers, the Dirac cones, due to their location at the K and K' points,

have a threefold symmetry like in graphene. It means that related bands have zero curvature not only along a line parallel to the $\Gamma \to K$ ($\Gamma \to K'$) direction, but also along lines obtained by rotating these lines with 120° and 240°. Similar with graphene, the two sub-lattice of the honeycomb symmetry ($p6m$) has same chemical environment, which can be responsible for the presence of Dirac cones at K points in TM-monolayers [14] [29]. To examine the carrier mobility around Dirac cones, the Fermi velocities are evaluated by linear fitting about the first derivatives of the band energies in Dirac points, namely, $v_F = \hbar \frac{\partial E}{\partial k}$ in linear band dispersion. Results show that all TM-monolayers have direction-dependent Dirac cones: Fermi velocities from $K \to \Gamma$ and $K \to M$ exhibit anisotropy. The first derivatives of related band energies in reciprocal space of TM-monolayers are from ± 8 to ± 16 eVÅ, compared to ± 34 eVÅ in graphene when approaching a Dirac point on lines through $K \to \Gamma$ and $K \to M$. The calculated Fermi velocities of TM-monolayers near Dirac point are from 0.2×10^6 to 0.5×10^6 m/s, which can be comparable to many other two dimensional nanomaterials [30-32].

Apart from high performance Dirac points in TM-monolayer, another important property is that three pristine TM-monolayers exhibit intrinsic magnetic because of the asymmetry of spin-up and spin-down states. To further understand the mechanism of magnetic couplings, two possible initial magnetic configurations for 2×2 supercell TM-monolayers are considered and examined. One is FM state (↑↑↑↑) and the other is AFM state (↑↓↑↓), the energy difference between FM and AFM states expressed as $E_{\text{ex}} = E_{FM} - E_{AFM}$, is used to access the magnetic interactions. Our results listed in

Table 1 demonstrate that TM-monolayer (TM = Ti, Zr, Hf) display FM ground states with magnetic moments 4, 2, 2 μ_B, respectively, V-monolayer exhibits AFM ground states, while for the other TM-monolayers (TM = Nb, Ta) are nonmagnetic with $E_{ex} = 0$.

3.3 Strain dependence

According to above analysis, FM couplings and Dirac points' behavior have been predicted theoretically in pristine TM-monolayers (TM= Ti, Zr, Hf), especially in the Hf-monolayer synthesized experimentally [22]. Yet, advanced applications often require materials with magnetic properties and high Fermi velocities which can be deliberately modulated in a well-controlled manner. Introducing strain is always an important technology in nanosystems. Previous studies indicated that increasing strain can enhance the FM order in fluorinated BN nanotubes [33, 34]. Moreover, magnetic couplings of pristine VS_2 and VSe_2 monolayers can also be tuned regularly by strain [16]. Therefore, the strain effects by varying the isotropic strain to make the honeycomb plane symmetries maintain are examined. The isotropic strain is defined as $\varepsilon = \Delta c / c_0$, where the lattice constants of the freestanding and strained supercell are equal to c_0 and $c = \Delta c + c_0$, respectively [35, 36]. Take Hf-monolayer as an example, the magnetic moments and Fermi velocity-related linear band slope changed by isotropic strain from -5% to 5% have been discussed in Figure 4. It shows that the magnetic moment per Hf atom and slope near Dirac point can be deliberately modulated by introducing strain effect. Besides, we also apply anisotropic strain in Hf-monolayer. As a result, Dirac point can be destroyed because of spatial symmetry

breaking. It is a strong evidence to verify that hexagonal symmetry is a main precondition for the presence of Dirac cones in TM-monolayers mentioned above.

3.4 Curie's temperature evaluation

The results above demonstrate TM-monolayers (TM = Ti, Zr, Hf) show ferromagnetism. For further applications, it is meaningful to explore and understand the magnetism change with temperature of these novel 2D TM monolayer [37, 38]. Curie's temperature (T_c) is a phase transition critical point of the system between ferromagnetism and paramagnetism states and is an important parameter to evaluate magnetic properties and applicable conditions of systems. To evaluate the Curie's temperatures of the TM monolayer, one simple but powerful model in statistical physics, Ising model, is used, which does not consider the magnetic anisotropy and quantum fluctuations as Heisenberg model. The Hamiltonian can be written as $\hat{H} = J\sum_{i,j} \mathbf{m}_i \cdot \mathbf{m}_j$, where $\mathbf{m}_i$ and $\mathbf{m}_j$ are the magnetic moments at sites i and j, J is the exchange parameter. The value of J is determined from the exchange energy ΔE ($\Delta E = E_{FM} - E_{AFM}$) by equation $J = \frac{1}{8} \cdot \frac{E_{ex}}{2m^2}$, where $m = |m|$ and the factor of $\frac{1}{8}$ is adopted because there are altogether eight magnetic coupling interactions in one (2×2) supercell. Here, take the synthesized structure Hf-monolayer as an example, the exchange parameter of Hf-monolayer is estimated to be -4.18 meV. With the help of above physical parameters, we applied the mean field theory (MFT), which is known as an efficient way to investigate the Curie temperature of the specific system, to evaluate the magnetic properties of Hf-monolayer. The partition function can be investigated by considering all possible

configurations according to the spin multiplicity of Hf-monolayer. As the magnetic moment of Hf-monolayer in the unit cell is 2 μ_B, the possible values of m are 2, 0, -2. And then the Curie's temperature T_c was obtained by determining the bifurcation critical point of the ensemble-average magnetic moment $\overline{m}$. The details are displayed as follows. The partition function can be written as

$$Z = \sum_{m=2,0,-2} e^{\lambda J m\overline{m}/k_B T} = 2\cosh\frac{2\lambda J\overline{m}}{k_B T} + 1$$

Where $\lambda = 6$ is the coordination number of the unit. Therefore, the average spin of each magnet is

$$\overline{m} = \frac{1}{Z}\left(\sum_{m=2,0,-2} m e^{\lambda J m\overline{m}/k_B T}\right) = \frac{4\sinh p\overline{m}}{2\cosh p\overline{m} + 1} \quad \left(p = \frac{2\lambda J}{k_B T}\right)$$

The average magnetism is the weight average of magnetism on each unit cell. It can be easily deduced that the when the parameter p changes, the static solution $\overline{m}$ varies, and the critical point is $p_c = 3/8$ corresponding with $T_c = 775K$. This corresponds to the phase transition of the system between ferromagnetism and paramagnetic states, which occurs at T_c.

However, it will overestimate T_c because of its neglection of the individual fluctuation. Thus, we further use 2D Ising model along with Monte Carlo (MC) simulations for more precise estimation, which is a common method for stochastic processes in statistical physics. Next, we perform MC simulations of the magnetic moment as a function of temperature in order to obtain T_c more precisely. In the MC simulations, an 100×100 supercell is used, and the calculation lasted for 8×10^6 loops. In each loop, the spins on all the sites in the supercell changed according to the spin states of Hf-monolayer. The results of the MC simulations are shown in Figure 5. It

can be seen that the magnetic moment per unit cell starts dropping dramatically from 2 μ_B at 420 K, the paramagnetic state is achieved at a temperature about 600 K (Curies' temperature) for Hf-monolayer. The temperature is reduced by 22.5% relative to MFT estimate mentioned above. The Curie's temperature of other ferromagnetic TM-monolayers (TM = Ti, Zr) are also discussed by MC simulations and listed in Table 2. The values of T_c for TM-monolayers (TM = Ti, Zr, Hf) are relatively higher than room temperature, which indicate that these 2D nanomaterials can maintain high spin polarization at room temperature or even much higher. In fact, TM-monolayers are quite comparable to the traditional ferromagnets such as Fe, Co, Ni or diluted magnetic semiconductors [39].

IV. Conclusion

Systematic first-principles calculations are carried out to study the electronic and magnetic properties of novel honeycomb TM-monolayers. Striking highlights of our investigation can be summarized into the flowing main points:

(1) The Optimized and freestanding TM-monolayers exhibit planar honeycomb symmetries. Band structures show that all of them are metallic and have Dirac points near Fermi level. Different with previous p-type Dirac points, Dirac points formed by d electrons in TM-monolayers can turn a new page for spintronic materials.

(2) The main precondition of the existence for Dirac points depends on spatial symmetry. Fermi velocities near Dirac points of TM-monolayers are estimated to be from 0.2×10^6 to 0.5×10^6 m/s, which can make a considerable contribution to high performance nanoelectronics.

(3) Magnetic moments and energy difference between different magnetic couplings are explored in detail. Results reveal that TM-monolayers (TM = Ti, Zr, Hf) are ferromagnetic, carrying magnetic moments 4, 2, and 2 μ_B per unit cell, respectively. V-monolayer is antiferromagnetic, while others are paramagnetic.

(4) Isotropic strain from -5% to 5% for Hf-monolayer can modulate the magnetic moments to some extent. Moreover, the first derivative of band energies near Dirac cones in reciprocal space will increase apparently with squeezing Hf-monolayer lattice, which obtains higher Fermi velocities.

(5) Last but not least, Curie's temperatures of ferromagnetic TM-monolayers (TM = Ti, Zr, Hf) have been simulated by both mean field theory and Monte Carlo approaches. High Curie's temperatures 580, 1180, and 600 K are obtained for TM-monolayers (TM = Ti, Zr, Hf), respectively. It indicates that TM-monolayers can maintain high spin polarization at room temperature.

Generally, we have investigated electronic and magnetic properties of novel TM monolayers by spin-polarized DFT. The intriguing Dirac points formed by *d* electrons with high performance in both spin-up and spin-down states provide a new platform in 2D systems. Moreover, the magnetic moments and carrier mobility can be tuned by experimentally achievable isotropic strains without breaking Dirac cones. It is noteworthy that study of Curie's temperatures provide strong guidance for further experiments and applications. It is worth to mention that substrates can affect on both geometric structures and electronic properties of the TM-monolayers. The existence of substrates can even enhance the stability of monolayers. Furthermore, hence the

planar Hf monolayer without bulking have been synthesized on substrate Ir (111) [21], we firmly believe that this kind of novel TM-monolayers will have bright future in nanotechnology.

Acknowledgment

This work is supported by the National Basic Research Program of China (973 program, 2013CB632401), National Natural Science foundation of China under Grant, 21333006 and 11174180, and the Fund for Doctoral Program of National Education 20120131110066. We also thank the National Supercomputer Center in Jinan for providing high performance computation.

Notes and References

[1] K. S. Novoselov, A. K. Geim, S. Morozov, D. Jiang, Y. Zhang, S. Dubonos, Grigorieva, and A. Firsov, Science, **306**, 666 (2004).

[2] K. Novoselov, E. McCann, S. Morozov, V. I. Fal'ko, M. Katsnelson, U. Zeitler, D. Jiang, F. Schedin, and A. Geim, Nat. Phys., **2**, 177 (2006).

[3] Y. Zhang, Y.-W. Tan, H. L. Stormer, and P. Kim, Nature, **438**, 201 (2005).

[4] H. Okamoto, et al., J. Am. Chem. Soc., **132**, 2710 (2010).

[5] Y. Ma, Y. Dai, and B. Huang, J. Phys. Chem. Lett. 4, 2471 (2013).

[6] Q. Tang, Y. Li, Z. Zhou, Y. Chen, and Z. Chen, ACS Appl. Mater. Interfaces, **2**, 2442 (2010).

[7] B. Radisavljevic, A. Radenovic, J. Brivio, V. Giacometti, and A. Kis, Nat. Nanotechnol., **6**, 147 (2011).

[8] D. Elias, R. Nair, T. Mohiuddin, S. Morozov, P. Blake, M. Halsall, A. Ferrari, D.

Boukhvalov, M. Katsnelson, and A. Geim, Science, **323**, 610 (2009).

[9] K. Novoselov, A. K. Geim, S. Morozov, D. Jiang, M. K. I. Grigorieva, S. Dubonos, and A. Firsov, Nature, **438**, 197 (2005).

[10] L. Ponomarenko, F. Schedin, M. Katsnelson, R. Yang, E. Hill, K. Novoselov, and A. Geim, Science, **320**, 356 (2008).

[11] K. K. Gomes, W. Mar, W. Ko, F. Guinea, and H. C. Manoharan, Nature, **483**, 306 (2012).

[12] X.-L. Qi and S.-C. Zhang, Rev. Mod. Phys., **83**, 1057 (2011).

[13] S. Cahangirov, M. Topsakal, E. Aktürk, H. Şahin, and S. Ciraci, Phys. Rev. Lett., **102**, 236804 (2009).

[14] D. Malko, C. Neiss, F. Viñes, and A. Görling, Phys. Rev. Lett., **108**, 086804 (2012).

[15] D. Yu, E. M. Lupton, M. Liu, W. Liu, and F. Liu, Nano Res., **1**, 56 (2008).

[16] J. Shen, Y. Hu, M. Shi, N. Li, H. Ma, and M. Ye, J. Phys. Chem. C, **114**, 1498 (2010).

[17] Y. Ma, Y. Dai, M. Guo, C. Niu, Y. Zhu, and B. Huang, ACS Nano, **6**, 1695 (2012).

[18] K. Xu, P. Chen, X. Li, C. Wu, Y. Guo, J. Zhao, X. Wu, and Y. Xie, Angew. Chem. Int. Ed. **52**, 10477 (2013).)

[19] M. Abel, S. Clair, O. Ourdjini, M. Mossoyan, and L. Porte, J. Am. Chem. Soc., **133**, 1203 (2010).

[20] Z. Shi, J. Liu, T. Lin, F. Xia, P. N. Liu, and N. Lin, J. Am. Chem. Soc., **133**,

6150 (2011).

[21] A. Krasheninnikov, P. Lehtinen, A. Foster, P. Pyykkö, and R. Nieminen, Phys. Rev. Lett., **102**, 126807 (2009).

[22] L. Li, Y. Wang, S. Xie, X.-B. Li, Y.-Q. Wang, R. Wu, H. Sun, S. Zhang, and H.-J. Gao, Nano Lett., **13**, 4671 (2013).

[23] H. Duan, N. Yan, R. Yu, C.-R. Chang, G. Zhou, H.-S. Hu, H. Rong, Z. Niu, J. Mao, H. Asakura, Nat. Commun. **5**,3093 (2014)

[24] J. P. Perdew, K. Burke, and M. Ernzerhof, Phys. Rev. Lett., **77**, 3865 (1996).

[25] G. Kresse and J. Furthmüller, Phys. Rev. B, **54**, 11169 (1996).

[26] G. Kresse and D. Joubert, Phys. Rev. B, **59**, 1758 (1999).

[27] H. J. Monkhorst and J. D. Pack, Phys. Rev. B, **13**, 5188 (1976).

[28] Y. Ma, Y. Dai, M. Guo, C. Niu, and B. Huang, J. Phys. Chem. C, **116**, 12977 (2012).

[29] V. M. Pereira, A. H. Castro Neto, and N. M. R. Peres, Phys. Rev. B **80**, 045401 (2009).

[30] C.-C. Liu, W. Feng, and Y. Yao, Phys. Rev. Lett., **107**, 076802 (2011).

[31] Y. Fan, M. Zhao, Z. Wang, X. Zhang, and H. Zhang, Appl. Phys. Lett., **98**, 083103 (2011).

[32] N. Drummond, V. Zolyomi, and V. Fal'Ko, Phys. Rev. B, **85**, 075423 (2012).

[33] F. Li, Z. Zhu, X. Yao, G. Lu, M. Zhao, Y. Xia, and Y. Chen, Appl. Phys. Lett., **92**, 102515 (2008).

[34] J. Zhou, Q. Wang, Q. Sun, and P. Jena, Phys. Rev. B, **81**, 085442 (2010).

[35] S.-M. Choi, S.-H. Jhi, and Y.-W. Son, Phys. Rev. B, **81**, 081407 (2010).

[36] M. Zhou, Y. Lu, C. Zhang, and Y. P. Feng, Appl. Phys. Lett., **97**, 103109 (2010).

[37] X. Li, J. Zhou, Q. Wang, Y. Kawazoe, and P. Jena, J. Phys. Chem. Let., 4, 259 (2012).

[38] J. Zhou and Q. Sun, J. Am. Chem. Soc., **133**, 15113 (2011).

[39] S.-D. Li, P. Chen, and B.-G. Liu, AIP Adv., **3**, 012107 (2013).

Table captions:

Table 1. Lattice parameters (Å), bond lengths (Å) and magnetic moments per unit cell (μ_B), ground states and energy difference between FM and AFM of TM (Ti, Zr, Hf, V, Nb, Ta)-monolayer and free standing graphene [28].

Table 2. Coupling parameters *J* (meV/μB), and Curies' temperatures (K) simulated by Monte Carlo.

Table 1. Lattice parameters (Å), bond lengths (Å) and magnetic moments per unit cell (μ_B), ground states and energy difference between FM and AFM of TM (Ti, Zr, Hf, V, Nb, Ta)-monolayer and free standing graphene [28].

Monolayer	Ti	Zr	Hf	V	Nb	Ta	graphene
Lattice parameter (Å)	4.41	4.69	4.88	4.29	4.25	4.32	2.45
Bond length (Å)	2.54	2.70	2.81	2.48	2.44	2.49	1.41
Magnetic moment (μ_B)	4	2	2	0	0	0	0
ΔE (meV)	-699.9	-552.6	-267.6	735	0	0	0
Ground States	FM	FM	FM	AFM	NM	NM	NM

Table 2. Coupling parameters J (meV/μB), and Curies' temperatures (K) simulated by Monte Carlo.

TM-monolayer	Ti	Zr	Hf
J (meV/μ_B^2)	-2.73	-8.63	-4.18
M (μ_B)	4	2	2
T_c (K)	580	1180	600

Figure captions:

Figure 1. Geometric structures of TM-monolayers (TM = Ti, Zr, Hf, V, Nb, Ta) in top and side views. The rhombus primitive cell is labeled with golden line. The orientations of primitive cell basis vectors **a** and **b** is also represented, respectively.

Figure 2. Corresponding Band structures of TM-monolayers. Orange lines represent spin-down states, while blue lines represent spin-up states. Horizontal dashed lines indicate Fermi levels. Dirac points are stressed out with black circles.

Figure 3. (a) Dirac cones formed by spin-down states in Hf-monolayer. (b) Corresponding partial density of states for d orbitals of spin-down states in Hf-monolayer. (c) The hexagon represents first Brillouin zone with letters designating special points and with the black lines along which the band structure display.

Figure 4. Strain dependence of the magnetic moment per Hf atom and slope associated with Fermi velocity near Dirac point.

Figure 5. Variation of the total magnetic moment per unit cell of 2D hf-monolayer with respect to the temperature.

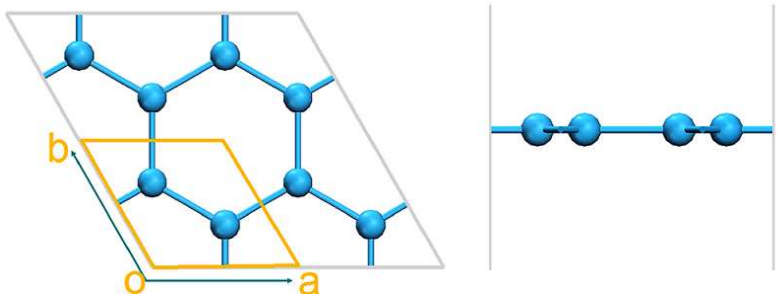

Figure 1. Geometric structures of TM-monolayers (TM = Ti, Zr, Hf, V, Nb, Ta) in top and side views. The rhombus primitive cell is labeled with golden line. The orientations of primitive cell basis vectors **a** and **b** is also represented, respectively.

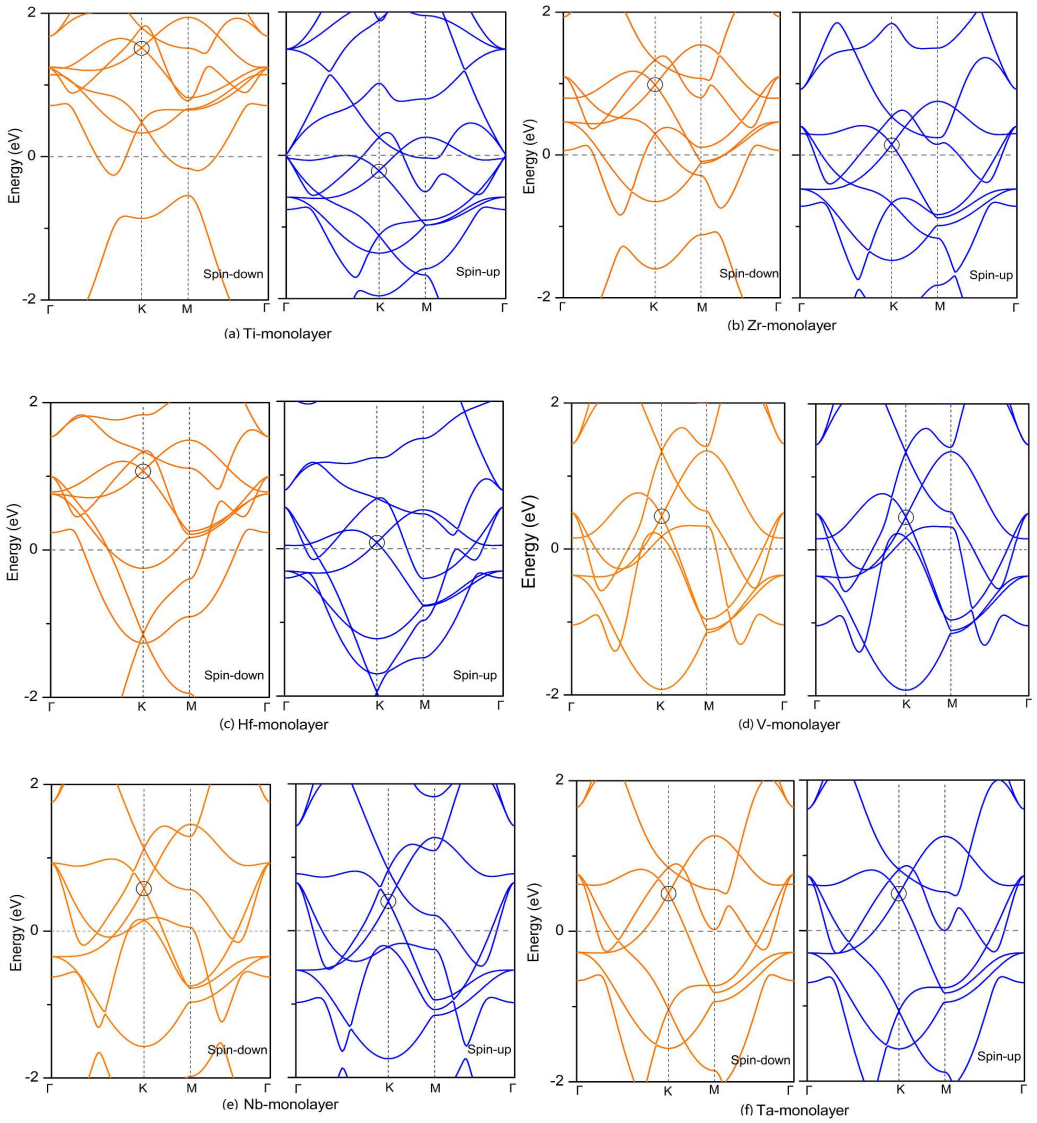

Figure 2. Corresponding Band structures of TM-monolayers. Orange lines represent spin-down states, while blue lines represent spin-up states. Horizontal dashed lines indicate Fermi levels. Dirac points are stressed out with black circles.

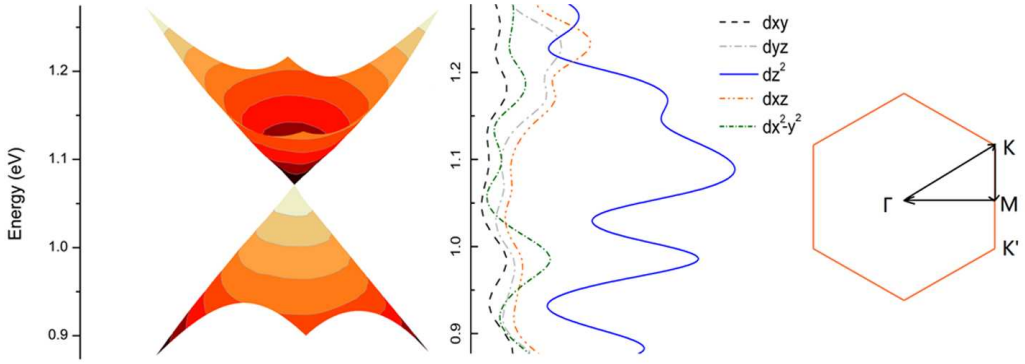

Figure 3. (a) Dirac cones formed by spin-down states in Hf-monolayer. (b) Corresponding partial density of states for d orbitals of spin-down states in Hf-monolayer. (c) The hexagon represents first Brillouin zone with letters designating special points and with the black lines along which the band structure display.

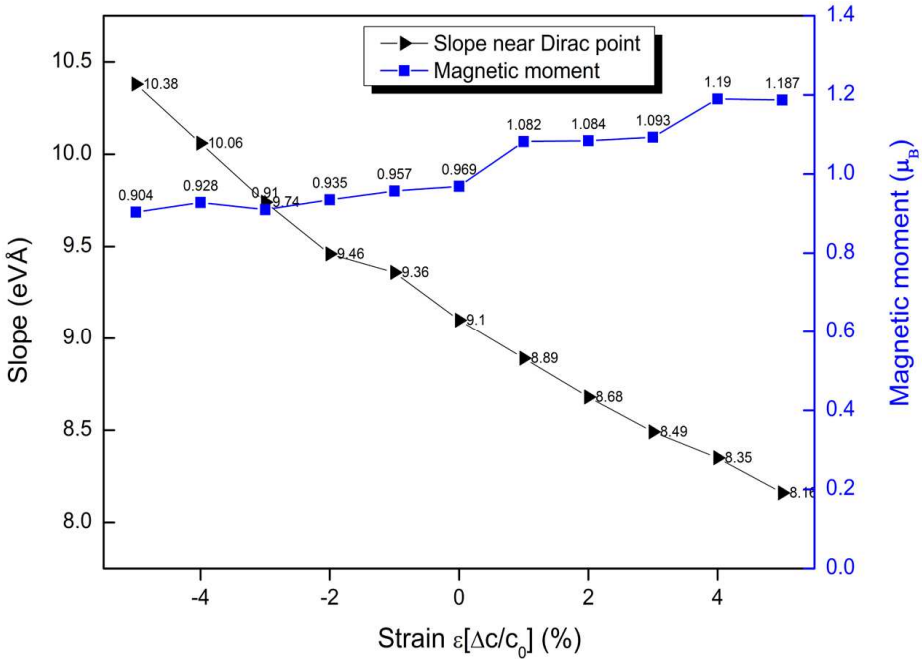

Figure 4. Strain dependence of the magnetic moment per Hf atom and slope associated with Fermi velocity near Dirac point.

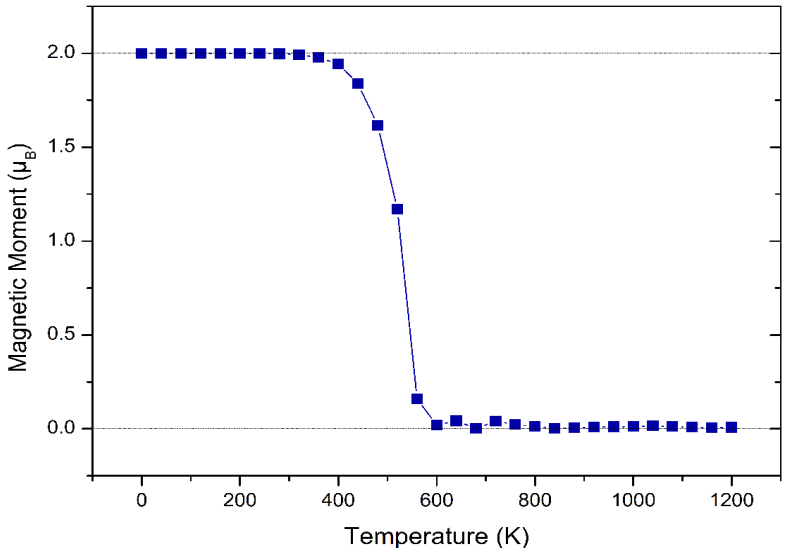

Figure 5. Variation of the total magnetic moment per unit cell of 2D hf-monolayer with respect to the temperature.